MESO-MECHANICAL MODELLING OF THIN ADHESIVE LAYERS

Tobias Andersson and Kent Salomonsson
University of Skövde
Box 408, SE-541 28 Skövde
tobias.andersson@ite.his.se kent.salomonsson@ite.his.se

Abstract

A meso-mechanical finite element model for a thin adhesive layer is developed. The model is calibrated to experimental results where the adhesive layer is loaded in monotonically increasing peel or shear, *cf.* Andersson and Stigh [1] and Alfredsson *et al.* [2], and to an *in situ* SEM study of the fracture process. The purpose of the meso-mechanical finite element model is to facilitate the development of constitutive laws for adhesive layers.

Ideas developed by Needleman [3], where structural continuum elements are bonded by cohesive elements are used as a basis for the finite element mesh. This thus enables micro cracks to propagate along the finite element boundaries.

The simulations are found to be in good agreement with the experiments. The model is also capable of reproducing realistically the deformation observed in both peel [1] and shear [2] experiments.

1. Introduction

Methods to develop phenomenological constitutive models are today usually based on methods by which the parameters of a given model are determined by comparisons with experimental data. Classically, the experimental data are confined to simple loading cases; most often simple tension or, more exclusively, tension in combination with torsion. More recently, methods have been developed where the experimental response of a structure is compared to results of simulations. The constitutive parameters are then selected to achieve good agreement with the experiments. Both methods suffer from shortcomings. The classical method can only capture the behaviour in a limited number of load combinations. The more exclusive experiments are also expensive and time-consuming. The newer methods, based on the study of the response of a structure, most often appear to be non-sensitive to small variations of the parameters to be determined. Moreover, the parameters determined to achieve good results for a limited number of experiments might not be appropriate in general. Relevant to the present study, are the papers by Yang *et al.* [4,5,6]. In these papers, a constitutive model for an adhesive layer is assumed. The model contains a number of free parameters that are chosen to give good agreement with some experiments.

Alternatively to these methods are the ones developed by modelling the relevant deformation and fracture mechanisms working on a microscopic length scale. The classical methods are based on the assumption that similar mechanisms work on the microscale as on the macro-scale as in Xia and Hutchinson [7]. In that paper, the shear stress – shear deformation relation for an adhesive layer is calculated from assumptions for the criteria for the nucleation and growth of micro-cracks. A shortcoming is that the authors have to, *a priori*, assume a distribution of nucleation spots for the micro-cracks. The criteria for crack growth and crack path selection are the same as used for macroscopic cracks in small scale yielding.

The resulting constitutive response is not satisfying as compared with experimental results; as soon as the micro-cracks nucleate, they cease to be in equilibrium and propagate to a position close to the adherends. The resulting shear stress – shear deformation relation drops vertically. This is not seen in experiments. An unsuccessful effort to remedy this by including non-linear material is reported by Strand [8]. In experiments, micro-cracks initiate and grow in a stable manner, *cf.* Andersson and Biel [9]. The resulting shear stress *vs*. shear deformation relation shows a long stable tail where the stress gradually decreases to zero, *cf.* [2]. It should be noted that in some situations, the structural response is insensitive to the shape of the stress – deformation relation and only the area under this curve (*i.e.* the fracture energy) influence the response, *cf.* [1]. It is thus easy to make improper deductions on the role of the constitutive behaviour based on the response of specific structures.

The purpose of this paper is to develop a meso mechanical finite element model to facilitate the development of constitutive laws for an adhesive layer. The idea is illustrated in Fig. 1. A representative volume element (RVE) is developed for which a number of parameters are to be determined. The RVE is subjected to pure peel (tension) and pure shear and the parameters of the model are determined by calibrating them to experimental results for these two special cases. In addition, once the parameters are determined, the RVE can be subjected to any load/unloading combination and the results can be used as additional data for the development of constitutive laws for the adhesive layer.

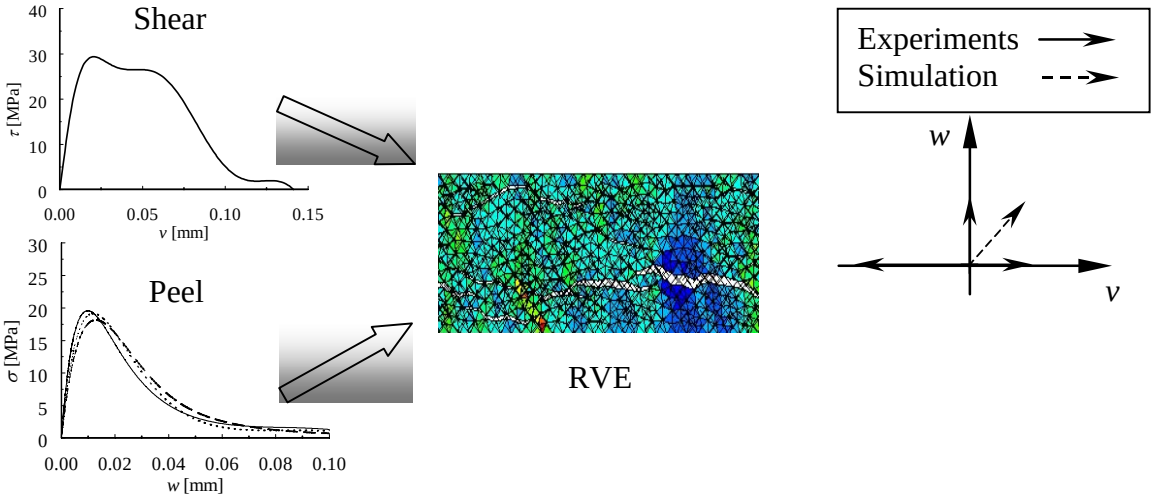

FIGURE 1. Mesomechanical strategy. Experimental data from [1], [9], [2] and [10] are used to calibrate the mesomechanical model. Simulations on the model are used in the development of a constitutive law for the adhesive layer.

2. Mesomechanical model

2.1 SEM-study

To investigate the behaviour of the adhesive (Betamate XW-1044-3, DOW Automotive) on a meso scale, an *in situ* peel test is performed in a SEM. Two different substances are easily identified in the SEM-images. These are identified as an epoxy/thermoplastic blend and a mineral compound, *cf.* Fig. 2. The epoxy/thermoplastic blend appears slightly darker than the mineral in these images.

The mineral occupies about 25 % of the volume. The mineral appears in clusters surrounded by the polymer blend. Thus, the polymer acts as a matrix and the mineral clusters as particles in a composite. The *in situ* study is set up using a small T-peel specimen with an adhesive layer thickness of 0.2 mm. Due to the design of the T-peel specimen, the adhesive

layer experiences almost pure tension. Due to a relatively high stiffness of the adherends, initiation of micro cracks occurs along a considerable part of the adhesive layer. The micro cracks appear to initiate in and around the more brittle areas, *i.e.* the areas identified as the mineral. Specifically, micro-cracks are observed to initiate in the larger clusters of mineral. After initiation and growth inside the clusters, the micro-cracks propagate through the epoxy matrix and coalesce to form macroscopic cracks, *cf.* Fig 2b. When the micro-cracks have been initiated, the mineral cluster dissolves into an extremely complex structure, *cf.* Fig 3.

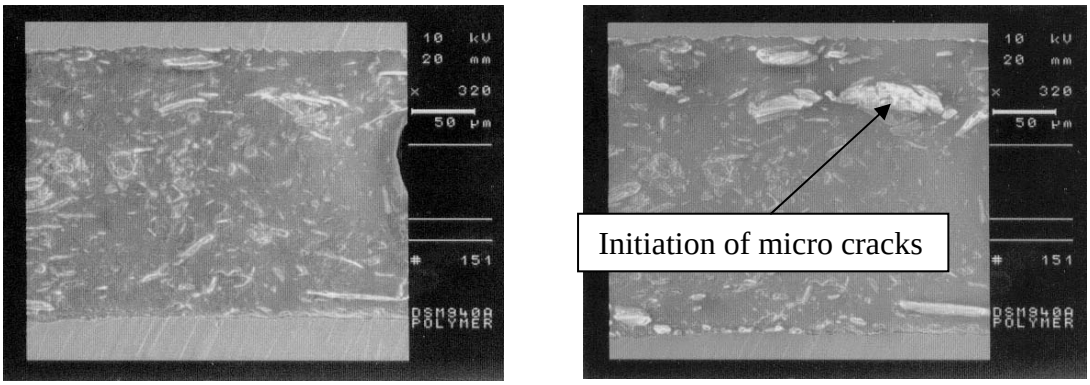

(a) (b)

FIGURE 2. SEM-images of the (a) initial configuration and (b) stretched configuration (about 12 % strain in the vertical direction).

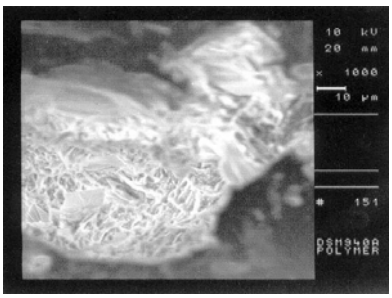

FIGURE 3. A SEM-image of the deformed mineral compound structure.

2.2 The representative volume element

A RVE shall represent the most likely structure to be found in the adhesive layer on a meso scale. To this end, the differences in intensity in the SEM-images are used to identify the different areas of the adhesive layer. With a given finite element mesh, the elements that fall within the brighter areas of the image are given the properties of the mineral and the elements that fall within the darker areas are given the epoxy/thermoplastic properties, *cf.* Fig. 4. The adhesive thickness is about 0.2 mm in the experiments and this thickness is kept in the RVE. The RVE shall at least contain two larger clusters of mineral. The length of the RVE is therefore set to 0.8 mm corresponding to four times the thickness of the adhesive layer. It should be noted that the method used here to develop a RVE does not reproduce the correct volume fraction of mineral since only a limited sample of the adhesive layer is used. However, since the RVE is rather large, the volume fraction varies only slightly with the choice of SEM-image.

3 Numerical model

To simplify the calculations, the RVE is assumed to be in a state of a plane stress. Considering the constraints of the adherends, it appears more realistic to use a state of plane deformation. However, in this initial study, numerical problems prevented us from achieving convergent results in plane deformation. The macroscopic deformation of an adhesive layer is typically of the same order of magnitude as the thickness of the layer, *cf.* [1] and [2]. Thus, it is important to consider large deformations in the numerical analysis. However, the local strain is not large and small strain formulations for the constitutive behaviour of the continuum elements are assumed adequate.

Two different types of elements are used in the finite element mesh; the continuum is modelled with triangular three-node elements. To enable crack propagation four-node interface elements are coupled between all the continuum elements. Thus, cracks are free to nucleate and propagate along the finite element boundaries. The number of initiation sites and the available propagation directions are obviously limited. However, if a large number of elements are used, this limitation is a minor problem. Different constitutive properties are used for the elements in the polymer blend and in the mineral, both for the continuum elements and for the interface elements. The interface elements at the interfaces between the mineral clusters and the polymer blend is given the same constitutive properties as the elements in the polymer blend.

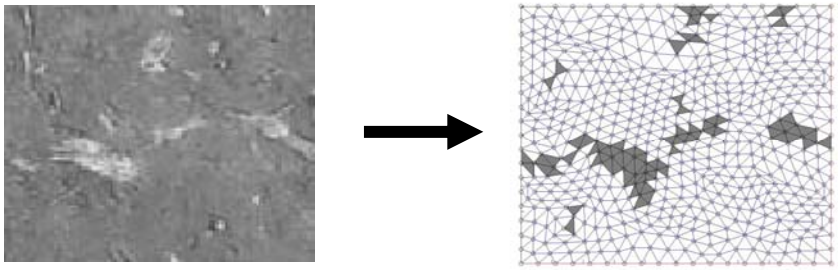

FIGURE 4. Schematic of identification of different substances and a FE-model.

3.1 Material model for the continuum elements

The polymer blend is modelled as a linear elastic material with linear isotropic hardening. Young's modulus for the polymer blend is E^{ep} = 2 GPa, where the superscript ep is used to denote the polymer blend; superscript m is used for the mineral. The yield strength, σ_Y^{ep}, is set to 50 MPa and the hardening modulus is assumed to be 100 MPa. The mineral compound is modelled as linearly elastic with Young's modulus E^{m} = 15 GPa. Poissons ratio is set to 0.4 for all continuum elements.

3.2 Material model for the interface elements

The properties of the interface elements are modelled using the model of Tvergaard and Hutchinson [11] as a basis. In this model, the fracture process is characterised by the phenomenological traction *vs*. generalised separation relation, *cf*. Fig. 5.

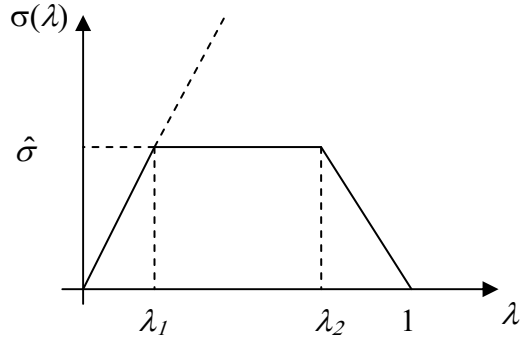

FIGURE 5. Traction *vs*. generalised separation relation for the interface elements.

The curve is defined by three parameters, a maximum stress $\hat{\sigma}$ and the two shape-parameters λ_1 and λ_2. The generalised separation λ is defined by

$$\lambda = \sqrt{\left(\frac{\delta_n}{\delta_n^c}\right)^2 + \left(\frac{\delta_t}{\delta_t^c}\right)^2} \tag{1}$$

where δ_n and δ_t are the relative displacements in peel and shear respectively. The superscript c indicates the critical separation. A potential $\Phi(\lambda)$ is introduced through

$$\Phi(\lambda) = \delta_n^c \int_0^\lambda \sigma(\lambda') \quad d\lambda' \tag{2}$$

The peel stress, σ_n, and the shear stress, σ_t, are derived from the potential, *viz*.

$$\sigma_n = \frac{\partial \Phi(\lambda)}{\partial \delta_n} = \frac{\sigma(\lambda)}{\lambda}\frac{\delta_n}{\delta_n^c} \qquad \sigma_t = \frac{\partial \Phi(\lambda)}{\partial \delta_t} = \frac{\sigma(\lambda)}{\lambda}\frac{\delta_n^c \delta_t}{\delta_t^{c\,2}} \tag{3a, b}$$

Thus, the model contains five parameters, $\lambda_1, \lambda_2, \delta_n^c, \delta_t^c$ and $\hat{\sigma}$, that fully describe the behaviour of an interface element.

In the experiments, unloading from severely deformed and deteriorated states is observed. Thus, it is necessary to adjust the Tvergaard-Hutchinson model to allow for different behaviour in loading and unloading. This is done by introducing a damage variable, ω, in the interface model, *i.e.*

$$\sigma(\lambda, \omega) = (1-\omega)\frac{\lambda}{\lambda_1}\hat{\sigma} \tag{4}$$

With a monotonically increasing λ, ω evolves according to

$$\omega(\lambda) = 1 - \frac{\lambda_1}{\lambda}\frac{\sigma(\lambda)}{\hat{\sigma}} \tag{5}$$

where $\sigma(\lambda)$ is given in Fig. 5. Note the difference between eqs. (4) and (5). Equation (4) is valid for all load cases whereas eq. (5) is only valid if λ is monotonically increasing. Now, introduce a so-called damage stress $\Omega(\lambda) = k\lambda^2/2$, which controls the growth of damage in the model. Also, introduce a damage criterion

$$\Theta(\Omega, \omega) \equiv \Omega - g(\omega) \le 0 \tag{6}$$

The inequality is changed to an equality if damage is to evolve. The second term, $g(\omega)$, is a damage resistance function which controls the damage evolution. By the use of eq. (6) a law of damage evolution can be derived according to

$$\dot{\Theta}(\Omega,\omega) = \dot{\Omega} - \dot{g} = 0 \qquad \dot{\omega} = -\frac{\partial \Theta}{\partial \Omega}\dot{\mu} = -\dot{\mu} \tag{7a,b}$$

The dissipation of this model is given by $\Omega\dot{\omega}$, *cf.* Alfredsson and Stigh [12]. Thus, $\dot{\mu} \le 0$ in order to achieve a thermodynamically consistent model. The condition for damage evolution at the end of a time step is given by

$${}^{n+1}\Theta = {}^{n+1}\Omega - g\left({}^{n+1}\omega\right) = 0 \tag{8}$$

Expanding $g(\omega)$ in a Taylor series yields

$${}^{n+1}\Theta = {}^{n+1}\Omega - {}^{n}g + {}^{n}G\Delta\mu = 0 \tag{9}$$

where $G = \dfrac{\mathrm{d}g}{\mathrm{d}\omega}$. Denote the two first terms of Θ by

$${}^{n+1}\Theta^{\mathrm{e}} = {}^{n+1}\Omega - {}^{n}g \quad \Rightarrow \quad {}^{n+1}\Theta = {}^{n+1}\Theta^{\mathrm{e}} + {}^{n}G\Delta\mu = 0 \tag{10}$$

During damage evolution, ${}^{n+1}\Theta^{\mathrm{e}} > 0$. In this case, eq. (10) yields an approximate value of $\Delta\mu$ from the condition ${}^{n+1}\Theta = 0$, *viz.*

$${}^{n+1}\Theta^{\mathrm{e}} > 0 \quad \Rightarrow \quad \Delta\mu = -\frac{{}^{n+1}\Theta^{\mathrm{e}}}{{}^{n}G} \tag{11 a,b}$$

If ${}^{n+1}\Theta^{\mathrm{e}} \le 0$, unloading takes place and the values of μ and ω are kept constant. For the present model, the evolution of ω can be calculated directly. If damage grows, *i.e.* if ${}^{n+1}\Theta^{\mathrm{e}} > 0$, λ increases beyond any previously attained value. In this case, ω is determined directly by eq. (5). The parameters are here chosen by trial and error. The numerical performance of the model is very sensitive to the choice of the parameters. Table 1 gives the parameters used in this study.

TABLE 1. Parameter values.

Substance	λ_1	λ_2	$\delta_{\mathrm{n}}^{\mathrm{c}}$ [μm]	$\delta_{\mathrm{t}}^{\mathrm{c}}$ [μm]	$\hat{\sigma}$ [MPa]
Polymer blend	0.0018	0.015	50	55	23.1
Mineral	0.0001	0.008	80	70	17.2

4. Experiments *vs.* FE-simulations

The parameters are calibrated to experiments in peel, *cf.* [1] and [9] and shear, *cf.* [2] and [10]. A video-microscope has been used to study the deformation process in the experiments reported in [9] and [10]. Special consideration has been taken to imitate the behaviour of these experiments when choosing the parameters.

The RVE used in the simulations consists of 15342 continuum element and 22845 interface elements. The model contains more than 90 kDOF.

4.1 FE simulations and peel experiments

In the simulation of the behaviour in peel, the boundary conditions are for $x = 0$, l: $u_x = 0$ and for $y = 0$: $u_x = u_y = 0$. For the remaining boundary $y = h$: $u_x = 0$ and $u_y = w$. By taking the average of the nodal stresses in the y-direction at the upper boundary, the macroscopic stress σ is determined.

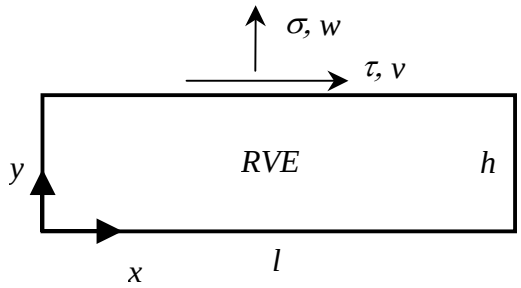

FIGURE 6. RVE in peel and shear.

Results from a typical experiment and a simulation are given in Fig. 7a. The result appears reasonably good. The simulation is also capable of mimicking most of the features observed in the experiments.

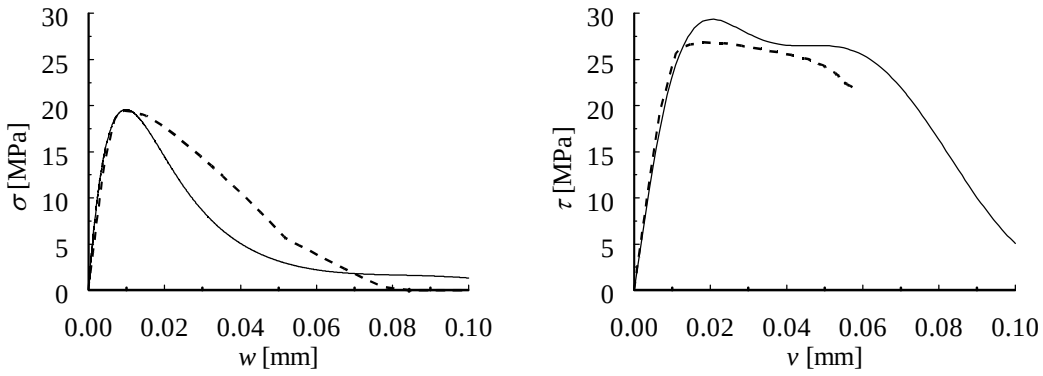

FIGURE 7. Comparisons between experiments (solid curves) and simulations (dashed curves). (a) Peel/DCB-results, (b) Shear/ENF-results.

4.2 FE simulations and shear experiments

In the simulation of the behaviour in shear, the boundary conditions are periodic in the horizontal direction *i.e.* $u_x(0,y) = u_x(l,y)$. For $y = 0$: $u_x = u_y = 0$ and for $y = h$: $u_x = v$ and $u_y =$ constant with zero resultant force in the vertical direction. Figure 7b shows that the FE-simulation is in good agreement with the experimental results. Note that the same RVE and parameters are used in the simulations in peel and shear.

Discussion and Conclusions

A basis for the development of a computational method for the prediction of the constitutive properties of adhesive layers has been presented. The basic idea is to use interface elements on the boundaries of the continuum elements. The adhesive is modelled on the meso level using a RVE, which is designed by the use of SEM-images. Due to the use of SEM images, the RVE provides a realistic material representation.

Several approaches have been made where interface elements are placed along a predefined crack propagation path. These approaches will in general not lead to a realistic behaviour, *cf.* Mishnaevsky and Schmauder [13]. However, in [3], the crack propagation path is not predefined but the continuum mesh is structured in such a way that it will lead to a longer crack path and a larger loss of energy. In the present paper the cracks have an almost entirely free crack propagation path, due to the unstructured mesh.

The FE-simulations are in good agreement with the experimental data. The model is also capable of reproducing realistically the deformation observed in both peel [1] and shear [2] experiments. In the future, a parameter study will be performed to achieve the optimal parameter settings.

Acknowledgement

We would like to thank the following persons; Dr. Björn Voigt, Mr. Robert Lillbacka and Dr. Magnus Ekh at Chalmers University of Technology, Gothenburg, Sweden for their help.

References

1. Andersson, T., and Stigh U., *Int J.Solids Structures*, vol. **41**, 413-434, 2003
2. Alfredsson, K. S., Biel, A., and Leffler, K., In: *9th International Conference on the Mechanical Behavior of Materials*, Geneva, Switzerland, 2003.
3. Needleman, A., *J. Appl. Mech.*, vol. **54**, 525-531, 1987
4. Yang, Q. D., Thouless, M. D., and Ward, S. M., *J. Mech. Phys. Solids*, vol. **47**, 1337-1353, 1999
5. Yang, Q. D., Thouless, M. D, and Ward, S. M., *Int J.Solids Structures*, vol. **38**, 3251-3262, 2001a
6. Yang, Q. D., Thouless, M. D, and Ward, S. M., *Int J.Fracture*, vol. **110**, 175-187, 2001b
7. Xia, Z. C., and Hutchinson, J. W., *Int J.Solids Structures*, vol. **8**, 1133-1148, 1994
8. Strand, N., *MSc. Thesis*, University of Skövde, Sweden, 1998.
9. Andersson, T., and Biel, A., Submitted to *The 15th European Conference of Fracture, Advanced Fracture Mechanics for Life and Safety Assessments*, Stockholm, Sweden, 2004.
10. Leffler, K., Alfredsson, K. S., Stigh, U., Submitted to *The 11th International Conference on Fracture*, Turin, Italy, 2005.
11. Tvergaard, V., and Hutchinson, J. W., *J. Mech. Phys. Solids*, vol. **40**, 1377-1397, 1992
12. Alfredsson, K. S., and Stigh, U., *Int J.Solids Structures*, In press, 2004
13. Mishnaevsky Jr, L. L, and Schmauder, S., *Appl. Mech. Rev.*, vol. **54**, no 1, 2001